# Axisymmetric, Primitive Equation, Spectral Tropical Cyclone Model. Part I: Formulation

WAYNE H. SCHUBERT

*Department of Atmospheric Science, Colorado State University, Fort Collins, CO 80523*

MARK DEMARIA

*National Center for Atmospheric Research,* Boulder, CO 80307*

(Manuscript received 23 April 1984, in final form 18 January 1985)

ABSTRACT

Beginning with the nine nonlinear governing equations for the simplest three-layer, axisymmetric, primitive equation, tropical cyclone model, we first introduce a vertical transform which decouples the linear part of the dynamics into three sets (one external, two internal modes) of three equations. After formulating a balance model boundary condition for each of the vertical modes, we introduce a radial transform based on normal modes. The radial transformation of the governing equations then gives spectral equations which describe the time evolution of the amplitude and phase of the external and internal geostrophic and gravity–inertia modes. A transform method for calculating the nonlinear and source/sink terms is described. As a simple test of the method, numerical integrations of the frictionless form of the nonlinear spectral equations with a specified heat source are made. The results illustrate the role of gravity–inertia waves in the forced transverse circulation and the quasi-gradient rotational flow. The model provides a simple framework in which to study the effects of friction and moist physics on nonlinear normal mode initialization procedures.

## 1. Introduction

In the early 1960s the mechanisms of tropical cyclone development were poorly understood. After many early difficulties, the first successful tropical cyclone simulations were made by Ooyama (1969a,b) using a three-layer axisymmetric balanced model and by Yamasaki (1968a,b) using a four-level axisymmetric primitive equation model. Encouraged by these results, many increasingly sophisticated models have been developed.[1] The tendency has been toward fully three-dimensional models with high horizontal and vertical resolution and more realistic "moist physics." An example of how far the modeling effort has progressed can be found in the genesis simulations of Kurihara and Tuleya (1981) and the movable nested-mesh vortex track predictions of Kurihara and Bender (1980). A common feature in all the tropical cyclone modeling literature to date is the use of finite difference methods.[2]

At the same time tropical cyclone modeling was rapidly advancing, global atmospheric modeling was experiencing the emergence of the spectral method. In particular, after the transform method of Orszag (1970) and Eliasen *et al.* (1970) had substantially increased the computational efficiency of spectral methods, there followed a period of rapid development of global shallow water equation spectral models (Bourke, 1972; Machenhauer and Rasmussen, 1972) and full primitive equation spectral models (Machenhauer and Daley, 1972; Bourke, 1974; Hoskins and Simmons, 1975). In many (but not all) respects these spectral models have outperformed finite difference models (e.g., Doron *et al.*, 1974; Simmons and Hoskins, 1975) and are presently being used in both research and operational work (e.g., the NCAR CCM and the ECMWF operational model).

One of the purposes of this study and its companion (DeMaria and Schubert, 1985) is to help answer the following question. To what extent can the spectral method be profitably applied to the tropical cyclone problem? Here we shall try to answer this question in the simplest context, i.e., with a physical model of maximum simplification. In most respects our model resembles that of Ooyama (1969a), which has the simplest geometry ($f$-plane, axisymmetric), the minimum vertical resolution (three layers), and the simplest moist physics. The major difference between our model and Ooyama's is our use of the primitive equations rather than the balance equations.

* The National Center for Atmospheric Research is sponsored by the National Science Foundation.

[1] A review of tropical cyclone modeling studies through the late 1970s can be found in Chapter 4 of Anthes (1982). A discussion of the conceptual difficulties encountered in these modeling efforts can be found in Ooyama (1982).

[2] The exceptions to this statement (in addition to the present paper) are the Fourier spectral model of DeMaria and Schubert (1984) and the cubic $B$-spline based, multiple nested, spectral model of Ooyama (1984).

One of the issues to be resolved in constructing a spectral model is the choice of basis functions. This depends on model geometry and boundary conditions. For global models, either spherical harmonics or Hough functions can be used. An advantage of using Hough functions (Kasahara, 1977, 1978) is that they are normal modes of the linearized equations on the sphere, which means that initialization is no longer a separate procedure but is built into the spectral model. In the axisymmetric hurricane model described here, a boundary condition appropriate for the balanced part of the flow will be used. With this boundary condition, the model normal modes can be used as basis functions, which makes the model a useful tool for studying hurricane initialization problems.

The outline of the present paper is as follows. In section 2 we present the nine governing equations for our three layer primitive equation model and then vertically transform these equations to obtain three coupled "shallow water" systems. We next develop (Section 3) the lateral boundary conditions which are applied to each shallow water system. In Section 4 the radial "normal mode" transform is introduced and the governing equations are transformed completely into spectral space. The details of the computational procedure are given in Section 5, and some numerical results are presented in Section 6. The paper concludes (Section 7) with a discussion of nonlinear normal-mode initialization and the various slow manifolds which can be studied with the present model.

## 2. Governing equations and vertical transform

We consider a model system which is axisymmetric and consists of three layers of homogeneous incompressible fluid. The thin bottom layer represents the PBL. The layers have densities $\rho_j = \epsilon_j \rho$ ($j = 0, 1, 2$ and $\epsilon_0 = 1$) with $\rho_0 > \rho_1 > \rho_2$ and thicknesses $H_j + h_j(r, t)$, where the constants $H_j$ are the undisturbed thicknesses at large radius. The fluid system is slightly more general than that of Ooyama (1969a), who assumed $h_0(r, t) = 0$ and $\rho_0 = \rho_1$.

Let $\phi_j$ ($j = 0, 1, 2$) denote the deviation of the geopotential of an isobaric surface from its standard value at large radius. The relation between the $\phi_j$ and the $h_j$ can easily be found from the hydrostatic equation. Introducing the vector notation $\mathbf{h} = [h_0, h_1, h_2]^T$ and $\boldsymbol{\phi} = [\phi_0, \phi_1, \phi_2]^T$, this relation can be written

$$\boldsymbol{\phi} = g\mathbf{E}\mathbf{h}, \tag{2.1}$$

where $g$ is the acceleration of gravity and

$$\mathbf{E} = \begin{pmatrix} 1 & \epsilon_1 & \epsilon_2 \\ 1 & 1 & \epsilon_2/\epsilon_1 \\ 1 & 1 & 1 \end{pmatrix}. \tag{2.2}$$

Equation (2.1) is required to change the mass continuity relation from an equation for $\mathbf{h}$ into an equation for $\boldsymbol{\phi}$ [see (2.5) below].

Defining $\mathbf{u} = [u_0, u_1, u_2]^T$ for the radial wind and $\mathbf{v} = [v_0, v_1, v_2]^T$ for the tangential wind, and with similar definitions for $\mathbf{a}$, $\mathbf{b}$, $\mathbf{c}$, $\mathbf{d}$, $\mathbf{f}$, $\mathbf{g}$, $\mathbf{q}$ and $\mathbf{s}$, we can write the radial wind, tangential wind and continuity equations in the vector form

$$\frac{\partial \mathbf{u}}{\partial t} - f(\mathbf{v} + \mathbf{b}) + \frac{\partial}{\partial r}(\boldsymbol{\phi} + \mathbf{c}) = \mathbf{f}, \tag{2.3}$$

$$\frac{\partial \mathbf{v}}{\partial t} + f(\mathbf{u} + \mathbf{a}) = \mathbf{g}, \tag{2.4}$$

$$\frac{\partial \boldsymbol{\phi}}{\partial t} + g\mathbf{E}\mathbf{H}\frac{\partial}{r\partial r}\{r(\mathbf{u} + \mathbf{d})\} = \mathbf{s}, \tag{2.5}$$

where

$$a_j = \frac{\zeta_j}{f} u_j, \quad \zeta_j = \frac{\partial r v_j}{r \partial r}, \quad b_j = \frac{\zeta_j}{f} v_j,$$

$$f_j = \{\epsilon_j(H_j + h_j)\}^{-1}\{(Q^+_{j-1/2} + \alpha_{j-1/2})(u_{j-1} - u_j) + (Q^-_{j+1/2} + \alpha_{j+1/2})(u_{j+1} - u_j)\},$$

$$c_j = \frac{1}{2}(u_j^2 + v_j^2),$$

$$g_j = \{\epsilon_j(H_j + h_j)\}^{-1}\{(Q^+_{j-1/2} + \alpha_{j-1/2})(v_{j-1} - v_j) + (Q^-_{j+1/2} + \alpha_{j+1/2})(v_{j+1} - v_j)\},$$

$$d_j = \frac{h_j}{H_j} u_j, \quad q_j = \epsilon_j^{-1}(Q_{j-1/2} - Q_{j+1/2}),$$

$$\alpha_{j-1/2} = \begin{cases} c_D(u_0^2 + v_0^2)^{1/2}, & j = 0 \\ \alpha, & j = 1 \\ \alpha, & j = 2 \\ 0, & j = 3, \end{cases}$$

$$Q_{j-1/2} = \begin{cases} 0, & j = 0 \\ Q^+_{1/2} - Q^-_{1/2}, & j = 1 \\ Q^+_{3/2} - Q^-_{3/2}, & j = 2 \\ 0, & j = 3 \end{cases}$$

and $\mathbf{s} = g\mathbf{E}\mathbf{q}$. The diagonal matrix $\mathbf{H}$ appearing in (2.5) is given by

$$\mathbf{H} = \begin{pmatrix} H_0 & 0 & 0 \\ 0 & H_1 & 0 \\ 0 & 0 & H_2 \end{pmatrix}. \tag{2.6}$$

In this layer model diabatic heating is represented by the upward vertical mass flux $Q^+_{j-1/2}$ and diabatic cooling by the downward flux $Q^-_{j-1/2}$. The difference between these two mass fluxes is the net diabatic flux $Q_{j-1/2}$. The momentum source/sink terms $f_j$ and $g_j$ both consist of a part due to diabatic mass fluxes and a part due to shearing stress (with constant coefficient

$\alpha$). At the surface the momentum fluxes are given by the standard drag coefficient formulation. The system of equations (2.3)–(2.5) is more general than that of Ooyama (1969a), who simplified (2.3) to the gradient wind relation and used a diagnostic version of the tangential wind equation in the planetary boundary layer. We are now ready to vertically transform the layer equations (2.3)–(2.5).

Our goal is to make the vertical structure problem involve the eigenvalues and eigenvectors of a symmetric, positive definite matrix.[3] We define the vertical transform of $\mathbf{u}$ by

$$\mathbf{U} = \mathbf{V}\mathbf{M}^{1/2}\mathbf{u}, \tag{2.7}$$

with similar definitions for $\mathbf{V}$, $\mathbf{\Phi}$, etc. The "mass matrix" $\mathbf{M}$ is defined by

$$\mathbf{M} = (H_0 + \epsilon_1 H_1 + \epsilon_2 H_2)^{-1} \begin{pmatrix} H_0 & 0 & 0 \\ 0 & \epsilon_1 H_1 & 0 \\ 0 & 0 & \epsilon_2 H_2 \end{pmatrix} \tag{2.8}$$

and the three-by-three "vertical transform" matrix $\mathbf{V}$ is as yet unspecified. Multiplying (2.3)–(2.5) first by $\mathbf{M}^{1/2}$ and then by $\mathbf{V}$ we obtain

$$\frac{\partial \mathbf{U}}{\partial t} - f(\mathbf{V} + \mathbf{B}) + \frac{\partial}{\partial r}(\mathbf{\Phi} + \mathbf{C}) = \mathbf{F}, \tag{2.9}$$

$$\frac{\partial \mathbf{V}}{\partial t} + f(\mathbf{U} + \mathbf{A}) = \mathbf{G}, \tag{2.10}$$

$$\frac{\partial \mathbf{\Phi}}{\partial t} + g\mathbf{V}\mathbf{A}\mathbf{V}^{-1} \frac{\partial}{r\partial r}\{r(\mathbf{U} + \mathbf{D})\} = \mathbf{S}. \tag{2.11}$$

where $\mathbf{A} = \mathbf{M}^{1/2}\mathbf{E}\mathbf{H}\mathbf{M}^{-1/2}$. Using (2.2), (2.6) and (2.8) we can easily show by matrix multiplication that

$$\mathbf{A} = \begin{pmatrix} H_0 & (\epsilon_1 H_0 H_1)^{1/2} & (\epsilon_2 H_0 H_2)^{1/2} \\ (\epsilon_1 H_0 H_1)^{1/2} & H_1 & \left(\frac{\epsilon_2}{\epsilon_1} H_1 H_2\right)^{1/2} \\ (\epsilon_2 H_0 H_2)^{1/2} & \left(\frac{\epsilon_2}{\epsilon_1} H_1 H_2\right)^{1/2} & H_2 \end{pmatrix}. \tag{2.12}$$

Since the matrix $\mathbf{A}$ is symmetric, its eigenvalues are real. In addition, its eigenvectors are real, orthogonal and form a complete set. The three two by two subdeterminants formed by striking the same row and column from $\mathbf{A}$ are all positive provided $1 > \epsilon_1 > \epsilon_2$. Thus, as long as the fluid is stably stratified, $\mathbf{A}$ is positive definite. This guarantees that the eigenvalues of $\mathbf{A}$ are positive.

[3] The analysis given here for our layered model is similar in certain respects to that given by Kasahara and Shigehisa (1983) and Temperton (1984) for a vertically staggered discretized atmospheric model.

We now construct $\mathbf{V}$ out of the eigenvectors of $\mathbf{A}$. Let $\mathbf{x}^{(k)}$ be the normalized eigenvector of $\mathbf{A}$ with associated eigenvalue $\bar{h}_k$, i.e.

$$\mathbf{A}\mathbf{x}^{(k)} = \bar{h}_k \mathbf{x}^{(k)}, \quad k = 0, 1, 2 \tag{2.13}$$

with

$$[\mathbf{x}^{(k)}]^{\mathrm{T}}\mathbf{x}^{(l)} = \begin{cases} 1, & k = l \\ 0, & k \neq l. \end{cases} \tag{2.14}$$

Let the three rows of $\mathbf{V}$ consist of the three eigenvectors $\mathbf{x}^{(0)}$, $\mathbf{x}^{(1)}$, $\mathbf{x}^{(2)}$. Because of (2.14) $\mathbf{V}^{\mathrm{T}}\mathbf{V} = \mathbf{I}$ (identity matrix) so that $\mathbf{V}$ is orthogonal and $\mathbf{V}^{-1} = \mathbf{V}^{\mathrm{T}}$. It then follows that

$$\mathbf{V}\mathbf{A}\mathbf{V}^{-1} = \begin{pmatrix} \bar{h}_0 & 0 & 0 \\ 0 & \bar{h}_1 & 0 \\ 0 & 0 & \bar{h}_2 \end{pmatrix}, \tag{2.15}$$

which simplifies (2.11) considerably.

We can now summarize by writing (2.9)–(2.11) in component form as

$$\frac{\partial U_m}{\partial t} - f(V_m + B_m) + \frac{\partial}{\partial r}(\Phi_m + C_m) = F_m, \tag{2.16}$$

$$\frac{\partial V_m}{\partial t} + f(U_m + A_m) = G_m, \tag{2.17}$$

$$\frac{\partial \Phi_m}{\partial t} + \bar{c}_m^2 \frac{\partial}{r\partial r}\{r(U_m + D_m)\} = S_m, \tag{2.18}$$

where $\bar{c}_m^2 = g\bar{h}_m$ and $m = 0, 1, 2$. For definiteness we arrange the eigenvalues of $\mathbf{A}$ such that $\bar{h}_0 > \bar{h}_1 > \bar{h}_2$. Then $h_0$ corresponds to the external mode and $\bar{h}_1$, $\bar{h}_2$ to the first and second internal modes, respectively. In practice the eigenvalues and normalized eigenvectors of $\mathbf{A}$ are computed numerically after the specification of the relative densities ($\epsilon_1$, $\epsilon_2$) and the layer thicknesses ($H_0$, $H_1$, $H_2$).

In Section 4 we shall find it convenient to write (2.16)–(2.18) in the vector form

$$\frac{\partial \mathbf{W}_m}{\partial t} + \mathbf{L}_m \mathbf{W}_m = \mathbf{N}_m + \mathbf{F}_m, \tag{2.19}$$

where

$$\mathbf{W}_m = [U_m, V_m, \Phi_m]^{\mathrm{T}},$$

$$\mathbf{N}_m = -\left[-fB_m + \frac{\partial C_m}{\partial r}, fA_m, \bar{c}_m^2 \frac{\partial r D_m}{r\partial r}\right]^{\mathrm{T}},$$

$$\mathbf{F}_m = [F_m, G_m, S_m]^{\mathrm{T}},$$

and

$$\mathbf{L}_m = \begin{pmatrix} 0 & -f & \frac{\partial}{\partial r} \\ f & 0 & 0 \\ \bar{c}_m^2 \frac{\partial r(\ )}{r\partial r} & 0 & 0 \end{pmatrix}.$$

We now wish to transform (2.19) in the radial direction. But, before doing so, we need to specify the lateral boundary conditions.

## 3. Boundary conditions

For computational efficiency we do not wish to extend the calculation beyond about 1000 km. Thus, although the physical problem provides us with no boundary condition at 1000 km, we are faced with the prospect of specifying one. We wish to apply a condition which simulates an infinite domain. Three possibilities are a wall, a gravity wave radiation condition and a balanced flow boundary condition.

### a. Problems with a wall

Perhaps the simplest possible condition is to require $U_m = 0$ at the lateral boundary $r = a$. This wall boundary condition is deficient in the sense that it distorts the "balanced response" unless it is applied at very large radius. To understand this point imagine the transverse circulation (low level inflow, upper level outflow) forced by a latent heat source which is confined within a radius of about 200 km. The transverse circulation projects onto both the external and internal modes, each of which decays with radius according to its Rossby length scale $\bar{c}_m/f$. Typical values of $\bar{c}_m/f$ for the external and internal modes (see Table 1) are 5700, 1000 and 600 km respectively. Thus, at a radius of 1000 km on an infinite domain, the transverse circulation associated with the first internal mode has decayed to roughly $1/e$ of its interior value, which implies considerable subsidence outside 1000 km. Placing a wall at 1000 km forces unrealistic subsidence inside 1000 km. An alternate statement of this deficiency is as follows. The wall boundary condition applied at 1000 km to the external and internal vertical modes will distort the solution all the way to the vortex center, perhaps not so much for the second internal mode, but for the first internal mode, and especially for the external mode. Another deficiency of the wall boundary condition is that it is a perfect reflector of gravity waves. We shall argue below that for a certain class of problems this second deficiency is not fatal.

### b. Gravity wave radiation condition versus balanced flow boundary condition

Based on the method of Bennett (1976), an exact boundary condition for the sum of the rotational and gravitational parts of the flow in an axisymmetric vortex has been derived by Hack and Schubert (1981, Section 5). The exact condition is complicated and cumbersome to apply (it is nonlocal in time). Two convenient limiting cases (see Eq. (5.7) and (5.8) of Hack and Schubert, 1981) of the exact condition occur when one considers the time scale of the motion compared to $f^{-1}$. For rapid motions one obtains an asymptotically valid radiation condition for pure gravity waves. For slow motions a balance type boundary condition results. Which of these two boundary conditions is more appropriate for the present model? The answer depends on which equation contains the dominant forcing and on the time and space scales of the forcing. For example, if the primary forcing appears as a mass source/sink in the continuity equation (2.18), and if this forcing occurs on a spatial scale much smaller than the Rossby radius of deformation and on a time scale much shorter than $f^{-1}$, then most of the excited energy will be in the form of gravity–inertia waves. The radiation condition is then most appropriate. However, if the time scale of the forcing is much longer than $f^{-1}$, most of the response will be of the geostrophic type, and the balance boundary condition is most appropriate. [Comparisons of the response of a slowly forced and a rapidly forced primitive equation model with a balanced model can be found in Schubert *et al.* (1980, Fig. 15).] In a tropical cyclone model with

TABLE 1. The specification of the parameters in the left column leads to the eigenvalues, eigenvectors, Rossby radii, boundary scales, and discrete wavenumbers given in the right column. The three rows of the matrix **V** give the eigenvectors of matrix **A**.

| | |
|---|---|
| $H_0 = 1725$ m | $\bar{c}_m = (g\bar{h}_m)^{1/2} = 287.3, 49.4, 32.3$ m s$^{-1}$, $m = 0, 1, 2$ |
| $H_1 = 3841$ m<br>$H_2 = 3212$ m | $\mathbf{V} = \begin{pmatrix} 0.4340 & 0.6691 & 0.6032 \\ 0.6039 & 0.2808 & -0.7460 \\ 0.6685 & -0.6881 & 0.2822 \end{pmatrix}$ external ($m = 0$)<br>first internal ($m = 1$)<br>second internal ($m = 2$) |
| $\epsilon_1 = 0.8982$<br>$\epsilon_2 = 0.8058$ | $\mu_m^{-1} = \dfrac{\bar{c}_m}{f} = 5746.0, 988.0, 646.0$ km, $m = 0, 1, 2$ |
| | $\lambda_m^{-1} = 19135.1, 1501.2, 873.4$ km |
| $f = 5.0 \times 10^{-5}$ s$^{-1}$ | |
| $a = 800$ km | $k_{mn}a = \begin{cases} 0.00, 2.42, 5.53, 8.66, 11.80, 14.93, \ldots, 146.87, & m = 0 \\ 0.00, 2.60, 5.61, 8.71, 11.84, 14.97, \ldots, 146.87, & m = 1 \\ 0.00, 2.71, 5.68, 8.76, 11.87, 14.99, \ldots, 146.88, & m = 2 \end{cases}$ |

parameterized moist physics we do not know *a priori* what the spatial and temporal behavior of the forcing is going to be. Thus, we cannot tell which boundary condition is most appropriate until we have some experience running the model. Using a three-dimensional Fourier spectral version of the present model DeMaria and Schubert (1984, Fig. 6) have found that during tropical cyclone simulations the amount of energy in either internal or external rotational modes is more than an order of magnitude larger than the energy in internal gravity waves and two orders of magnitude larger than that in external gravity waves. In addition, the gravity modes which are present do not combine to yield propagating wave trains but rather are nearly in balance with the nonlinear and forcing terms so that the model is evolving along the slow manifold (Leith, 1980). Based on this result we consider the balanced flow boundary condition most appropriate for the present model. Although the balanced flow boundary condition is also a perfect reflector of gravity waves, it is much preferable to the wall boundary condition because it allows a realistic transverse circulation at the boundary.

*c. Derivation of the balanced flow boundary condition*

To derive the balance boundary condition we simplify (2.16) to the geostrophic relation $fV_m = \partial\Phi_m/\partial r$ and use this result to eliminate $\Phi_m$ between (2.17) and (2.18). Then, assuming the nonlinear and forcing terms vanish for large $r$, we obtain

$$r\frac{\partial}{\partial r}\left(r\frac{\partial U_m}{\partial r}\right) - (\mu_m^2 r^2 + 1)U_m = 0 \quad \text{for large } r, \tag{3.1}$$

where $\mu_m = f/\bar{c}_m$. We can write the general solution of (3.1) as a linear combination of the first-order modified Bessel functions $I_1(\mu_m r)$ and $K_1(\mu_m r)$. Since $I_1(\mu_m r)$ grows with $r$, we set its coefficient to zero. The coefficient of $K_1(\mu_m r)$ is unknown but it can be eliminated by using the derivative relation

$$\frac{drK_1(\mu_m r)}{rdr} = -\mu_m K_0(\mu_m r)$$

to obtain

$$\frac{\partial rU_m}{r\partial r} + \lambda_m U_m = 0 \quad \text{at} \quad r = a, \tag{3.2}$$

where

$$\lambda_m = \frac{\mu_m K_0(\mu_m a)}{K_1(\mu_m a)}. \tag{3.3}$$

Equation (3.2) is the required boundary condition and is to be applied to each vertical mode $m = 0, 1, 2$.

## 4. Radial transform

Let us first consider the complex, three component vectors $\mathbf{p} = [p_0, p_1, p_2]^T$ and $\mathbf{q} = [q_0, q_1, q_2]^T$. The mode $m$ inner product of $\mathbf{p}$ and $\mathbf{q}$ is defined by

$$(\mathbf{p}, \mathbf{q})_m = \frac{2}{a^2}\int_0^a \left(p_0 q_0^* + p_1 q_1^* + \frac{1}{\bar{c}_m^2} p_2 q_2^*\right) rdr + \frac{2}{\lambda_m a}\left(\frac{1}{\bar{c}_m^2} p_2 q_2^*\right)_{r=a}. \tag{4.1}$$

Now let $\mathbf{K}_{mns}(r)$ be the complex, three component, time independent, normalized vector kernel given by

$$\mathbf{K}_{mns}(r) = A_{mns}\begin{cases}\begin{pmatrix} 0 \\ \bar{c}_m k_{mn} J_1(k_{mn} r) \\ -\bar{c}_m f J_0(k_{mn} r)\end{pmatrix}, & s = 0 \\ \begin{pmatrix} i\nu_{mns} J_1(k_{mn} r) \\ f J_1(k_{mn} r) \\ \bar{c}_m^2 k_{mn} J_0(k_{mn} r)\end{pmatrix}, & s = 1, 2,\end{cases} \tag{4.2}$$

where

$$A_{mns} = \left\{(\nu_{mns}^2 + f^2 + \bar{c}_m^2 k_{mn}^2)\left[\left(1 + \frac{2}{\lambda_m a}\right) \times J_0^2(k_{mn} a) + J_1^2(k_{mn} a)\right]\right\}^{-1/2}. \tag{4.3}$$

$J_0$ and $J_1$ are the order-zero and order-one Bessel functions of the first kind, $k_{mn}$ ($n = 1, 2, 3, \cdots$) are the discrete wavenumbers satisfying

$$k_{mn} J_0(k_{mn} a) + \lambda_m J_1(k_{mn} a) = 0, \tag{4.4}$$

and

$$\nu_{mns} = \begin{cases} 0, & s = 0 \\ -(f^2 + \bar{c}_m^2 k_{mn}^2)^{1/2}, & s = 1 \\ (f^2 + \bar{c}_m^2 k_{mn}^2)^{1/2}, & s = 2 \end{cases}. \tag{4.5}$$

Using the Bessel function derivative relations (A10) and (A11) of the Appendix, it can easily be shown that

$$\mathbf{L}_m \mathbf{K}_{mns} = i\nu_{mns}\mathbf{K}_{mns}. \tag{4.6}$$

As discussed in the Appendix, the basis functions (4.2) are orthonormal with respect to the inner product (4.1), i.e.

$$(\mathbf{K}_{mns}, \mathbf{K}_{mn's'})_m = \begin{cases} 1, & (n', s') = (n, s) \\ 0, & \text{otherwise.}\end{cases} \tag{4.7}$$

Using this orthonormality it is possible to write our radial transform pair as

$$\mathbf{W}_m(r, t) = \sum_{n=1}^{\infty}\sum_{s=0}^{2} W_{mns}(t)\mathbf{K}_{mns}(r), \tag{4.8}$$

$$W_{mns}(t) = (\mathbf{W}_m(r, t), \mathbf{K}_{mns}(r))_m, \tag{4.9}$$

where $W_{mns}(t)$ is a complex, scalar function of time. Equation (4.9) is the transformation from radial physical to spectral space, and (4.8) is the transformation back.

The spectral equations [i.e. the equations for $W_{mns}(t)$] are derived by first taking the inner product of (2.19) and $\mathbf{K}_{mns}(r)$ to obtain

$$\left(\frac{\partial \mathbf{W}_m}{\partial t}, \mathbf{K}_{mns}\right)_m + (\mathbf{L}_m\mathbf{W}_m, \mathbf{K}_{mns})_m = (\mathbf{N}_m, \mathbf{K}_{mns})_m + (\mathbf{F}_m, \mathbf{K}_{mns}). \quad (4.10)$$

Using the definition (4.1) and integrating the second term in (4.10) by parts we obtain

$$(\mathbf{L}_m\mathbf{W}_m, \mathbf{K}_{mns})_m = (\mathbf{W}_m, -\mathbf{L}_m\mathbf{K}_{mns})_m + \frac{2}{\lambda_m a}\left[\left(\frac{\partial r U_m}{r\partial r} + \lambda_m U_m\right)K^{(2)}_{mns} + \left(\frac{\partial r K^{(0)}_{mns}}{r\partial r} + \lambda_m K^{(0)}_{mns}\right)^* \Phi_m\right]_{r=a}, \quad (4.11)$$

where $K^{(0)}_{mns}$ and $K^{(2)}_{mns}$ are the first and last components of the vector $\mathbf{K}_{mns}$ defined by (4.2). The boundary term involving $U_m$ vanishes because of (3.2), while the boundary term involving $K^{(0)}_{mns}$ vanishes for $s = 0$ because of (4.2) and for $s \neq 0$ because of (4.4). Then, using (4.6) we can write

$$(\mathbf{L}_m\mathbf{W}_m, \mathbf{K}_{mns})_m = (\mathbf{W}_m, -i\nu_{mns}\mathbf{K}_{mns})_m = i\nu_{mns}(\mathbf{W}_m, \mathbf{K}_{mns})_m. \quad (4.12)$$

Equation (4.10) then becomes

$$\frac{dW_{mns}}{dt} + i\nu_{mns}W_{mns} = N_{mns} + F_{mns}, \quad (4.13)$$

where

$$N_{mns} = (\mathbf{N}_m, \mathbf{K}_{mns})_m \quad (4.14)$$

$$F_{mns} = (\mathbf{F}_m, \mathbf{K}_{mns})_m. \quad (4.15)$$

We have now transformed our original governing system (2.3)–(2.5) into the spectral equation (4.13). In the next section we shall summarize the computational steps which are necessary in the numerical time integration of (4.13).

## 5. Computational procedure

### a. Preliminaries

Our first task is to specify the constants $H_0$, $H_1$, $H_2$, $\epsilon_1$, $\epsilon_2$. This specification fixes the matrix $\mathbf{A}$ and hence the equivalent depths $\bar{h}_0$, $\bar{h}_1$, $\bar{h}_2$. Since we are trying to simulate a compressible fluid let us reverse the argument and consider $\bar{h}_0$, $\bar{h}_1$, $\bar{h}_2$ as given (from some compressible fluid model) and $H_0$, $H_1$, $H_2$, $\epsilon_1$, $\epsilon_2$ as quantities to be determined. Obviously two additional conditions are required. Here we obtain the additional relations by requiring that the percentages of basic state total column mass for layers 0, 1, 2 be $^2/_9$, $^4/_9$, $^3/_9$, respectively, i.e. $^9/_2\epsilon_0 H_0 = {}^9/_4\epsilon_1 H_1 = {}^9/_3\epsilon_2 H_2$. This can be interpreted as 200, 400 and 300 mb thick layers in a model bounded by the tropopause at 100 mb. Using the values of $\bar{c}_m = (g\bar{h}_m)^{1/2}$ given in the top row of Table 1 we then obtain the mean depths and density ratios given in the left column of the table. [These values of $\bar{c}_m$ have been chosen to be close to the first three eigenvalues given by Fulton and Schubert (1985) for a high resolution compressible fluid model with a mean tropical sounding and a lid at 100 mb.] Also shown in the table are the vertical transform matrix $\mathbf{V}$ (the rows of which are the eigenvectors of $\mathbf{A}$), the Rossby radii $\mu_m^{-1}$, the boundary scales $\lambda_m^{-1}$, and the discrete wavenumber spectrum obtained from the solution of (4.4). Here we have chosen $f = 5 \times 10^{-5}$ s$^{-1}$ (about 20°N) and $a = 800$ km. The gravity–inertia wave frequencies determined from (4.5) are displayed in Fig. 1. The first 48 values of $k_{mn}a$ for $m = 1$ are shown by the dots in Fig. 1.

### b. Nonlinear terms

The nonlinear and forcing terms ($N_{mns}$ and $F_{mns}$) which appear in (4.13) are calculated using the transform method (Orszag, 1970; Eliasen *et al.*, 1970). The first step is to apply the inverse radial transform (4.8) at specified radial grid points $r_k$. We then apply the inverse of the vertical transform which (see Equ. 2.7) is given by

$$\mathbf{u} = \mathbf{M}^{-1/2}\mathbf{V}^{-1}\mathbf{U}, \quad (5.1)$$

with similar expressions for $\mathbf{v}$, $\phi$, etc. In order to calculate the nonlinear products which appear in (2.3)–(2.5) at the physical space grid points $r_k$, radial derivatives of $\mathbf{u}$, $\mathbf{v}$ and $\phi$ are also needed. Equations (2.3)–(2.5) can be written in advective form so that the only required derivatives are $\partial ru_j/r\partial r$, $\partial rv_j/r\partial r$ and $\partial\phi_j/\partial r$. These can be calculated by first defining a vector $\mathbf{P}_m$ as

$$\mathbf{P}_m = \begin{pmatrix} \dfrac{\partial rU_m}{r\partial r} \\ \dfrac{\partial rV_m}{r\partial r} \\ \dfrac{\partial \Phi_m}{\partial r} \end{pmatrix}. \quad (5.2)$$

Now, taking $\partial r(\ )/r\partial r$ of the first two components of (4.8) and $\partial/\partial r$ of the third component and using (5.2), (A10)–(A11) gives

$$\mathbf{P}_m(r, t) = \sum_{n=1}^{\infty}\sum_{s=0}^{2} W_{mns}\mathbf{K}'_{mns}(r) \quad (5.3)$$

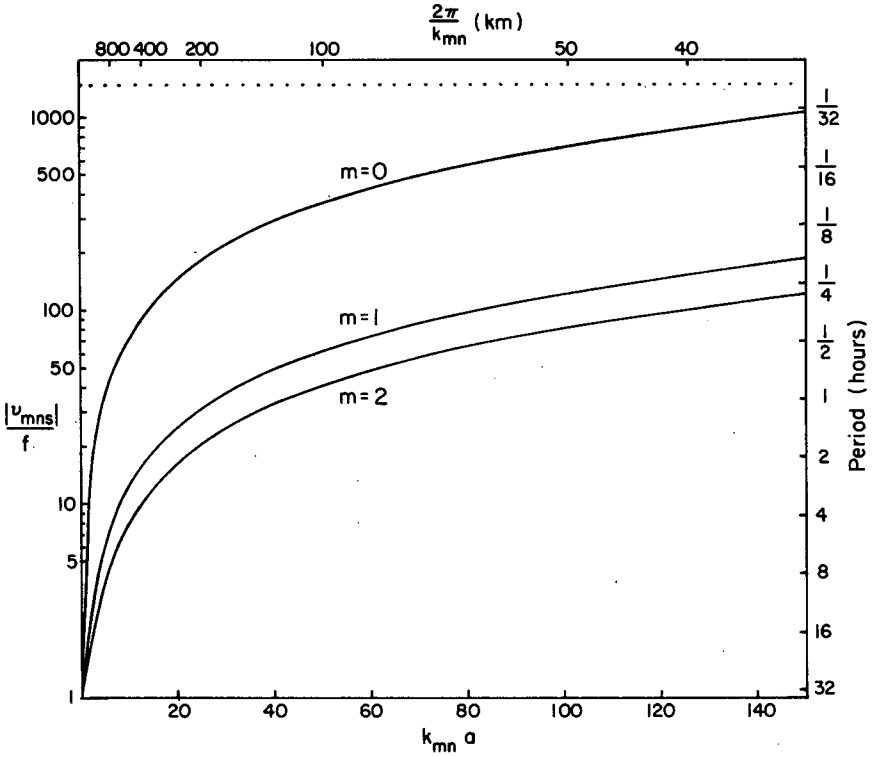


FIG. 1. The gravity–inertia wave frequencies determined from (5.5). Although continuous lines have been drawn, only discrete wavenumbers are allowed (see Table 1). The discrete wavenumbers determined from (5.4) for the first internal mode ($m = 1$) are indicated by the dots.

where $\mathbf{K}'_{mns}(r)$ is given by

$$\mathbf{K}'_{mns}(r) = k_{mn}A_{mns}\begin{cases}\begin{pmatrix}0\\ \bar{c}_m k_{mn}J_0(k_{mn}r)\\ \bar{c}_m f J_1(k_{mn}r)\end{pmatrix}, & s = 0\\ \begin{pmatrix}i\nu_{mns}J_0(k_{mn}r)\\ fJ_0(k_{mn}r)\\ -\bar{c}_m^{\,2}k_{mn}J_1(k_{mn}r)\end{pmatrix}, & s = 1, 2.\end{cases} \tag{5.4}$$

Then $\mathbf{P}_m$ at the physical space grid points $r_k$ can be calculated using (5.3). Applying the inverse transform (5.1) to the vectors made up of the components of (5.2) for $m = 0, 1, 2$ gives the required physical space derivatives.

The next step is to calculate all the nonlinear and source/sink terms in (2.3)–(2.5) at the physical space grid points $r_k$. Once this is done, the nonlinear and forcing terms are transformed in the vertical to give $\mathbf{N}_m$ and $\mathbf{F}_m$ which appear in (2.19).

The final step is to transform $\mathbf{N}_m$ and $\mathbf{F}_m$ in the radial direction using (4.14)–(4.15), where the integral which appears in the definition of the inner product (4.1) is evaluated using a numerical quadrature rule. Since the series expansion in (4.8) must be truncated at a finite number of terms ($n = N$), the quadratic nonlinear terms are represented by the product of two truncated Bessel series. The integrand in (4.14) is then represented by the product of the two truncated series with the Bessel functions from the kernel of the transform. In the Fourier–spectral model in cartesian geometry described in DeMaria and Schubert (1984), an analogous integral must be evaluated, where the integrand is the product of two Fourier series with a Fourier basis function. For the cartesian case, when the Fourier series are truncated at wavenumber $N$, the integrand can then be represented by a Fourier series with maximum wavenumber $3N$. It is then possible to evaluate the integral exactly using $3N + 1$ point trapezoidal quadrature, which prevents aliasing errors in the calculation of the spectral amplitudes of the quadratic nonlinear terms. For the model in cylindrical geometry, however, the product of the two truncated Bessel series with the Bessel function from the kernel of the transform cannot be represented by a Bessel series truncated at $3N$ terms. Thus, a quadrature rule cannot be developed which evaluates the integral in (4.14) exactly for quadratic nonlinear terms, and some aliasing error will occur. Since the Bessel functions $J_0$ and $J_1$ behave similar

to Fourier functions for large $r$, $3N + 1$ point trapezoidal quadrature was used to evaluate the integrals in (4.14)–(4.15). Thus, the physical space grid points $r_k$ are $3N + 1$ evenly spaced points between $r = 0$ and $r = a$.

In order to test the sensitivity of the solutions to the quadrature, we made several runs with a reduced number of quadrature points (between $2N + 1$ and $3N + 1$) for a simulation with a specified mass source/sink term. This resulted in only very small changes in the dependent variables at the end of a six-day integration. In addition, this same simulation was run using Simpson's rule with $3N + 1$ points to evaluate the nonlinear terms, and again only very small changes in the dependent variables resulted. Thus, the $3N + 1$ point trapezoidal quadrature appears to be adequate for the evaluation of the nonlinear terms.

### c. *Time differencing*

Since (4.13) is nonlinear, it is necessary to solve for $W_{mns}$ using time differencing. An advantage to writing the governing equations in the form of (4.13) is that the linear terms can be evaluated exactly by multiplying the equation by an integrating factor to give

$$\frac{d}{dt}(W_{mns}e^{i\nu_{mns}t}) = (N_{mns} + F_{mns})e^{i\nu_{mns}t}. \quad (5.5)$$

Letting $t = \tau\Delta t$ and using forward time differencing for the first time step and the second-order Adams-Bashforth scheme for all subsequent time steps gives

$$W^{(1)}_{mns} = [W^{(0)}_{mns} + \Delta t(N^{(0)}_{mns} + F^{(0)}_{mns})]e^{-i\nu_{mns}\Delta t}, \quad (5.6)$$

$$W^{(\tau+1)}_{mns} = W^{(\tau)}_{mns}e^{-i\nu_{mns}\Delta t} + \Delta t\left\{\frac{3}{2}[N^{(\tau)}_{mns} + F^{(\tau)}_{mns}]e^{-i\nu_{mns}\Delta t} - \frac{1}{2}[N^{(\tau-1)}_{mns} + F^{(\tau-1)}_{mns}]e^{-i\nu_{mns}2\Delta t}\right\}, \quad (5.7)$$

where the superscript indicates the time level. DeMaria and Schubert (1984) have shown that in a three-layer Fourier-spectral tropical cyclone model, the above time differencing scheme allows the use of a time step about 2.5 times larger than the explicit limit.

### d. *Summary of computational procedure*

In summary, the spectral equation (4.13) was solved using the time differencing scheme (5.6)–(5.7), where the nonlinear and forcing times $N_{mns}$ and $F_{mns}$ are calculated using the transform method. For the simulations presented in the next section, the series (4.8) was truncated at $N = 48$ and a 45 second time step was used. With this truncation and time step, a six day simulation required 172 seconds of computing time on the NCAR Cray-1.

## 6. Numerical results

As a simple test of the spectral method we have performed a numerical integration of the frictionless equations (i.e. $c_D = \alpha = 0$) with the specified forcing $Q^-_{1/2} = Q^-_{3/2} = 0$ and

$$Q^+_{3/2}(r, t) = \tilde{Q}(t)\left(\frac{r}{\tilde{r}}\right)^2 \exp\left[1 - \left(\frac{r}{\tilde{r}}\right)^2\right],$$

$$Q^+_{1/2}(r, t) = \left\{\frac{H_0 + h_0}{(H_0 + h_0) + \epsilon_1(H_1 + h_1)}\right\}Q^+_{3/2}(r, t),$$

where $\tilde{r} = 50$ km. The radial distribution of $Q^+_{3/2}$ is shown in Fig. 2. In order to minimize the excitation of transient waves, the time dependent part $\tilde{Q}(t)$, which is shown in Fig. 3a, has been chosen to be a smooth switch on to a steady state value. The steady state value is 0.15 m s$^{-1}$, which can be interpreted as corresponding to a horizontally averaged heating of about 15°C day$^{-1}$ inside 150 km.

The time evolution of the tangential wind in layer 1 is shown in Fig. 3b. After six days a vortex with 42 m s$^{-1}$ tangential wind at about 50 km radius has developed. The inner 400 km model structure for the vertical modes $U_m$, $V_m$, $\Phi_m$ ($m = 0, 1, 2$) at six days is shown in Fig. 4. The dominant contribution to the radial wind is from the first internal mode $U_1$, which leads to inflow in the lower two layers and outflow in the upper layer. In contrast, the dominant inner region contributions to the tangential wind and the geopotential are from the external mode (i.e. $V_0$ and $\Phi_0$). Outside 270 km $V_1$ becomes dominant, while outside 100 km $\Phi_1$ becomes dominant. The second internal mode $U_2$, $V_2$, $\Phi_2$ plays a minor role in this example. (When surface friction is included the second internal mode acquires a more important role.)

The inner 400 km model structure for layers 1 and 2 at six days is shown in Fig. 5. The fields for layer 0 are not shown since they are nearly identical to those for layer 1. The lower tropospheric peak inflow is 0.96 m s$^{-1}$ at about 80 km and the upper tropospheric peak outflow is 1.55 m s$^{-1}$ at about 100 km.

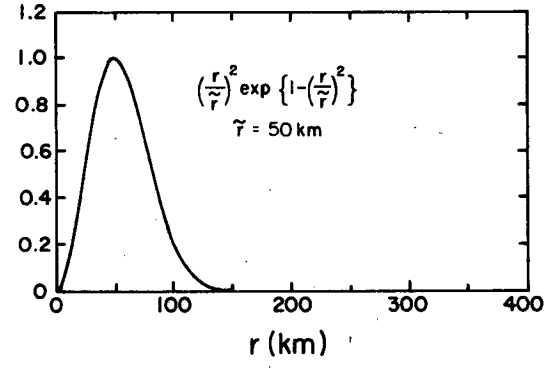


FIG. 2. Radial dependence of the specified "heating" $Q^+_{3/2}(r, t)$.

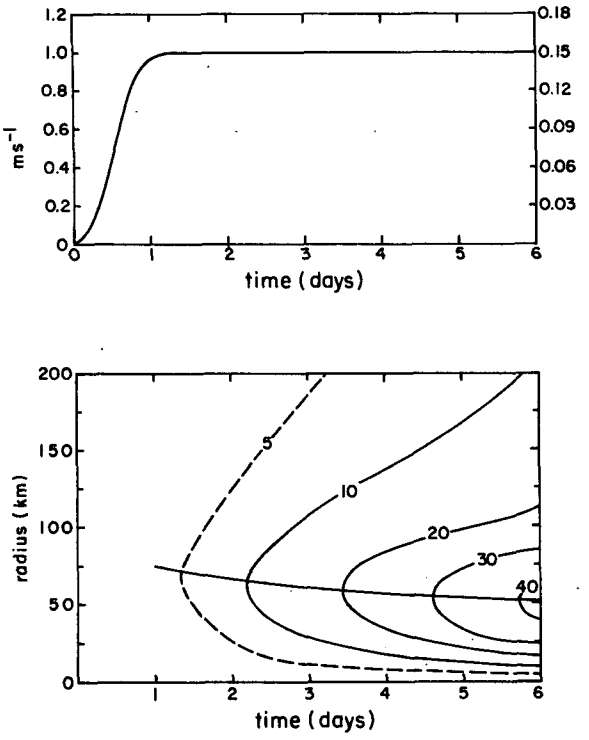


FIG. 3. At the top is shown the time dependent part of the forcing $\tilde{Q}(t)$, with the dimensional scale on the right. The steady state value of 0.15 m s$^{-1}$ corresponds to an average inner 150 km heating of about 15°C day$^{-1}$, or an average inner 250 km heating of about 5°C day$^{-1}$, which is a typical cloud cluster value. On the bottom are shown isolines of the tangential wind inside 200 km for layer 1.

Since the geostrophic mode has zero radial wind, both of the $u$ fields shown in the top of Fig. 5 are due entirely to gravity–inertia modes. The situation for the tangential wind is quite different. The $v$ fields shown in the middle part of Fig. 5 are due almost entirely to geostrophic modes, i.e. a very good approximation to $v$ can be obtained by summing (4.8) over the $s = 0$ modes only. At $r = 60$ km the gravity–inertia mode contribution to $v_1$ is $-0.26$ m s$^{-1}$ and to $v_2$ is 0.40 m s$^{-1}$. At all other radii the gravity–inertia mode contribution is of smaller magnitude. Finally, the geopotential field is due to both geostrophic and gravity–inertia modes, with the gravity–inertia modes giving most of the inner region structure. This is illustrated in the bottom of Fig. 5, where the solid lines are the actual fields and the dashed lines are the geostrophic mode contributions to the total. Note that the gravity–inertia mode contribution (the difference between the solid and dashed curves) is significant inside 150 km.

If the forcing continues, the tangential flow becomes more and more intense. But what happens if the forcing is now turned off? The results of such experiments (not shown) confirm that if the forcing is turned off slowly (in as smooth a fashion as it was turned on, say) very little transient gravity wave activity is excited and the fields of wind and geopotential look almost identical to Fig. 5 except that $u_j$ is essentially zero. It is as if the gravity–inertia wave spectrum is divided into three parts: a part which yields $v \approx 0$, $u \approx 0$, $\partial u/\partial t \approx 0$, $\phi \neq 0$ and is responsible for the cyclostrophic part of gradient wind balance; a part which yields $v \approx 0$, $u \neq 0$, $\partial u/\partial t \approx 0$, $\phi \approx 0$ and is responsible for the slowly changing transverse circulation; a part which yields $v \approx 0$, $u \neq 0$, $\partial u/\partial t \neq 0$, $\phi \neq 0$ and is responsible for transient gravity–inertia wave trains. In terms of Leith's (1980) slow manifold diagram, it is the first part which takes us from the geostrophic manifold to the "adiabatic, frictionless slow manifold" while it is the second part which then takes us to the "diabatic slow manifold." Although we often interpret balanced models of the type discussed by Schubert and Hack (1983) as not allowing gravity–inertia wave motion, these models are certainly capable of describing motions near the adiabatic or diabatic slow manifolds. Thus, balanced models can describe the first two parts of the gravity–inertia wave spectrum. It is only the third part of the spectrum which is filtered by the gradient balance approximation.

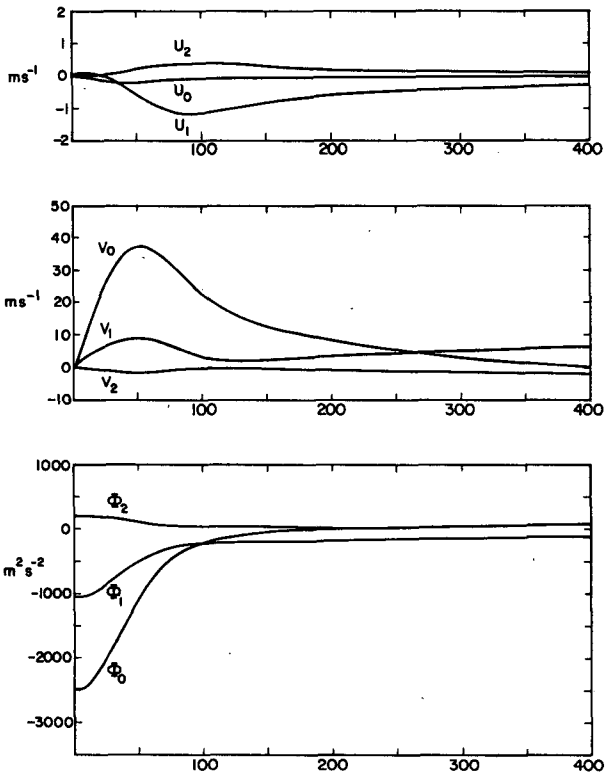


FIG. 4. Radial distributions of the vertical modes $U_m$, $V_m$, $\Phi_m$ ($m = 0, 1, 2$) at six days for the inner 400 km of the model domain.

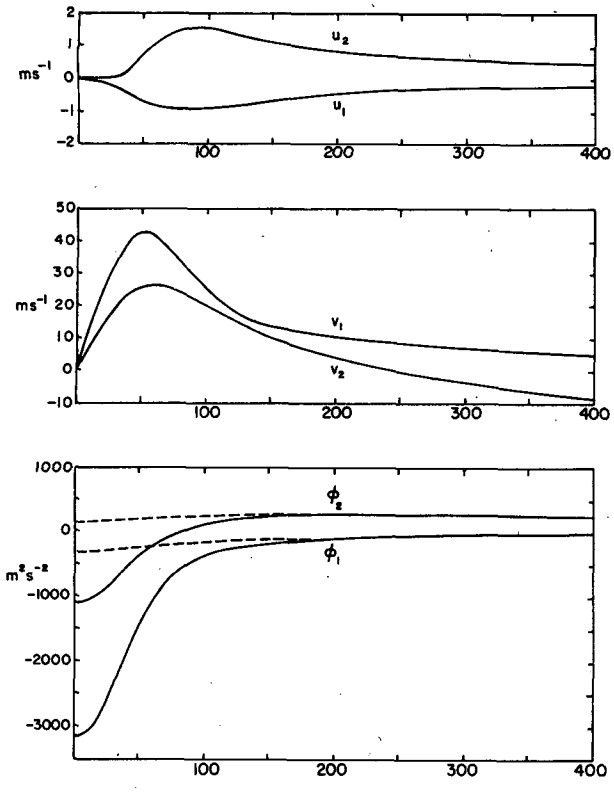


FIG. 5. Radial distributions (solid lines) of $u$, $v$ and $\phi$ at six days for layers 1 and 2. The dashed lines in the bottom panel are the geostrophic mode contributions to the total geopotential fields. Thus, the differences between the solid and dashed curves are the gravity–inertia mode contributions, which are quite significant in the inner region.

## 7. Concluding remarks

We have presented, in as simple a context as possible, a primitive equation spectral hurricane model. Our emphasis has been on the basic dynamical structure, and we have avoided a detailed discussion of parameterized moist physics. However, a time dependent moisture field (either in the boundary layer only or in both the lower two layers) and parameterized moist physics can be included along the lines described by Ooyama (1969a). The moisture field can be represented in terms of truncated Bessel series, but with different lateral boundary conditions and hence different wavenumber discretization. One shortcoming of the present model is its highly idealized vertical structure. The incorporation of a more realistic vertical structure can be accomplished in a variety of ways without changing the radial transform part of the analysis.

A potential use of the present spectral model is in illuminating problems with nonlinear normal-mode initialization in cases where curvature, friction and moist processes are all important. In the present model nonlinear normal-mode initialization is accomplished by neglecting $dW_{mns}/dt$ in (4.13) for the gravity–inertia modes ($s = 1, 2$), which results in the diagnostic equations

$$\left.\begin{aligned} W_{mn1} &= \frac{1}{iv_{mn1}}\left[N_{mn1}(W_{mn0}, W_{mn1}, W_{mn2}) + F_{mn1}(W_{mn0}, W_{mn1}, W_{mn2})\right] \\ W_{mn2} &= \frac{1}{iv_{mn2}}\left[N_{mn2}(W_{mn0}, W_{mn1}, W_{mn2}) + F_{mn2}(W_{mn0}, W_{mn1}, W_{mn2})\right] \end{aligned}\right\}. \quad (7.1)$$

In the unconstrained initialization procedure these nonlinear equations are iteratively solved for the gravity modes $W_{mn1}$ and $W_{mn2}$ while the geostrophic mode $W_{mn0}$ remains fixed. In the geopotential constrained initialization procedure the equations are solved iteratively while the geopotential remains fixed. Equations (7.1) constitute an approximation to the diabatic, frictional, slow manifold. If we neglect $F_{mn1}$ and $F_{mn2}$ in (7.1) we obtain an approximation to the adiabatic, frictionless, slow manifold. The convergence problems associated with geopotential constrained, adiabatic, frictionless, nonlinear normal mode initialization have been discussed by Tribbia (1981) and Daley (1980, 1981), who actually constructed the slow manifold diagram for a highly truncated barotropic vortex model. A similar construction of the slow manifold diagram is possible for the spectral hurricane model if the truncation is severe enough.

One obvious extension of the present model is to retain the cylindrical coordinate system and the $f$-plane approximation but relax the assumption of axisymmetry. It is then more convenient to work with the vorticity and divergence equations rather than the original momentum equations. The vertical transform is unchanged, and the derivation of balance type boundary conditions is similar to the discussion in Section 3 except that the conditions must be applied not only mode by mode in the vertical direction but also mode by mode in the tangential direction. The kernel of the radial transform is similar to (4.2) except that an additional index (tangential wavenumber) and Bessel functions of all orders (one for each tangential wavenumber) are involved. The final spectral equation is similar to (5.13) with the additional index for tangential wavenumber. This asymmetric spectral model is useful for studying certain aspects of the banded structure of hurricanes.

*Acknowledgments.* The authors are grateful to Scott Fulton for his invaluable advice. We also wish to thank Odilia Panella for her help in preparing the manuscript. This research was supported by NSF Grant ATM-8207563 and ONR Grant N00014-84-C-0591.

## APPENDIX

### Orthonormality of $K_{mns}(r)$

Here we wish to prove (4.7), a statement of the orthonormality of the basis functions (4.2) with respect to the inner product (4.1). We consider first the case where $s = 1$ or 2 and $s' = 1$ or 2, which allows us to write

$$(\mathbf{K}_{mns}, \mathbf{K}_{mn's'})_m = \frac{2}{a^2} A_{mns} A_{mn's'} \left\{ (\nu_{mns}\nu_{mn's'} + f^2) \times \int_0^a J_1(k_{mn}r) J_1(k_{mn'}r) r dr + \bar{c}_m^2 k_{mn} k_{mn'} \left[ \int_0^a J_0(k_{mn}r) J_0(k_{mn'}r) r dr + \frac{a}{\lambda_m} J_0(k_{mn}a) J_0(k_{mn'}a) \right] \right\}, \quad \text{(A1)}$$

which can be simplified as follows. Take the difference between $J_0(k_{mn}r)$ times the equation solved by $J_0(k_{mn'}r)$ and $J_0(k_{mn'}r)$ times the equation solved by $J_0(k_{mn}r)$, integrate by parts, and use the condition (4.4) to obtain

$$(k_{mn}^2 - k_{mn'}^2) \left[ \int_0^a J_0(k_{mn}r) J_0(k_{mn'}r) r dr + \frac{a}{\lambda_m} J_0(k_{mn}a) J_0(k_{mn'}a) \right] = 0. \quad \text{(A2)}$$

When $n' \neq n$, we have $k_{mn'} \neq k_{mn}$ and the bracketed term in (A2) must vanish. When $n' = n$, the integral in (A2) can be evaluated with the aid of the derivative relation

$$r J_0^2(kr) = \frac{d}{dr} \left\{ \frac{r^2}{2} [J_0^2(kr) + J_1^2(kr)] \right\} \quad \text{(A3)}$$

to obtain

$$\int_0^a J_0(k_{mn}r) J_0(k_{mn'}r) r dr + \frac{a}{\lambda_m} J_0(k_{mn}a) J_0(k_{mn'}a) = \begin{cases} \frac{a^2}{2} \left[ \left( 1 + \frac{2}{\lambda_m a} \right) J_0^2(k_{mn}a) + J_1^2(k_{mn}a) \right], & n' = n \\ 0, & n' \neq n. \end{cases} \quad \text{(A4)}$$

In a similar fashion, but with the aid of the derivative relation

$$r J_1^2(kr) = \frac{d}{dr} \left\{ \frac{r^2}{2} [J_1^2(kr) - J_0(kr) J_2(kr)] \right\} \quad \text{(A5)}$$

and the recurrence relation

$$J_0(kr) + J_2(kr) = \frac{2}{kr} J_1(kr), \quad \text{(A6)}$$

$$\int_0^a J_1(k_{mn}r) J_1(k_{mn'}r) r dr = \begin{cases} \frac{a^2}{2} \left[ \left( 1 + \frac{2}{\lambda_m a} \right) J_0^2(k_{mn}a) + J_1^2(k_{mn}a) \right], & n' = n \\ 0, & n' \neq n. \end{cases} \quad \text{(A7)}$$

Substitution of (A4) and (A7) into (A1) yields

$$(\mathbf{K}_{mns}, \mathbf{K}_{mn's'})_m = \begin{cases} 1, & (n's') = (n, s) \\ 0, & \text{otherwise} \end{cases} \quad \text{(A8)}$$

for $s = 1$ or 2 and $s' = 1$ or 2. Thus, we have proved orthonormality *within* the gravity-wave set. The proof of orthonormality within the geostrophic set proceeds in an analogous manner, with the result that (A8) also holds for $s = s' = 0$.

Finally, we consider the orthogonality of a basis function from the gravity wave set with the basis function from the geostrophic set, i.e., $s = 1$ or 2 and $s' = 0$. Then, instead of (A1), we obtain

$$(K_{mns}, K_{mn'0})_m = \frac{2}{a^2} A_{mns} A_{mn'0} f \bar{c}_m \left\{ k_{mn'} \int_0^a J_1(k_{mn}r) J_1(k_{mn'}r) r dr - k_{mn} \left[ \int_0^a J_0(k_{mn}r) J_0(k_{mn'}r) r dr + \frac{a}{\lambda_m} J_0(k_{mn}a) J_0(k_{mn'}a) \right] \right\}. \quad \text{(A9)}$$

Integrating the $J_1$ term by parts using the derivative relations

$$\frac{dJ_0(kr)}{dr} = -kJ_1(kr), \quad \text{(A10)}$$

$$\frac{drJ_1(kr)}{rdr} = kJ_0(kr), \quad \text{(A11)}$$

and the condition (4.4), it is possible to show that the right-hand side of (A9) vanishes. This completes the proof of (4.7).

## REFERENCES


Anthes, R. A., 1982: *Tropical Cyclones: Their Evolution, Structure and Effects. Meteor. Monogr.*, No. 41, Amer. Meteor. Soc., 208 pp. [ISBN 0-933876-54-8.]

Bennett, A. F., 1976: Open boundary conditions for dispersive waves. *J. Atmos. Sci.*, **33**, 176–182.

Bourke, W., 1972: An efficient, one-level, primitive equation spectral model. *Mon. Wea. Rev.*, **100**, 683–689.

——, 1974: A multi-level spectral model. I. Formulation and hemispheric integrations. *Mon. Wea. Rev.*, **102**, 687–701.

Daley, R., 1980: On the optimal specification of the initial state for deterministic forecasting. *Mon. Wea. Rev.*, **108**, 1719–1735.

——, 1981: Normal mode initialization. *Rev. Geophys. Space Phys.*, **19**, 450–468.

——, and W. H. Schubert, 1984: Experiments with a spectral tropical cyclone model. *J. Atmos. Sci.*, **41,** 901–924.

DeMaria, M., and W. H. Schubert, 1985: Axisymmetric, primitive equation, spectral, tropical cyclone model. Part II: Normal-mode initialization. *J. Atmos. Sci.*, **42,** 1225–1236.

Doron, E., A. Hollingsworth, B. J. Hoskins and A. J. Simmons, 1974: a comparison of grid point and spectral methods in a meteorological problem. *Quart. J. Roy. Meteor. Soc.*, **100,** 371–383.

Eliasen, E., B. Machenhauer and E. Rasmussen, 1970: On a numerical method for the integration of the hydrodynamical equations with spectral representation of the horizontal fields. Rep. No. 2, Kobenhavns Universitet, Institut for Teoretisk Meteorologi.

Fulton, S. R., and W. H. Schubert, 1985: Vertical normal mode transforms: theory and application. *Mon. Wea. Rev.*, **113,** 647–658.

Hack, J. J., and W. H. Schubert, 1981: Lateral boundary conditions for tropical cyclone models. *Mon. Wea. Rev.*, **109,** 1404–1420.

Hoskins, B. J., and A. J. Simmons, 1975: A multi-layer spectral model and the semi-implicit method. *Quart. J. Roy. Meteor. Soc.*, **101,** 637–655.

Kasahara, A., 1977: Numerical integration of the global barotropic primitive equations with Hough harmonic expansions. *J. Atmos. Sci.*, **34,** 687–701.

——, 1978: Further studies on a spectral model of the global barotropic primitive equations with Hough harmonic expansions. *J. Atmos. Sci.*, **35,** 2043–2051.

——, and Y. Shigehisa, 1983: Orthogonal vertical normal modes of a vertically staggered discretized atmospheric model. *Mon. Wea. Rev.*, **111,** 1724–1735.

Kurihara, Y., and M. A. Bender, 1980: Use of a movable nested-mesh model for tracking a small vortex. *Mon. Wea. Rev.*, **108,** 1792–1809.

——, and R. E. Tuleya, 1981: A numerical simulation study on the genesis of a tropical storm. *Mon. Wea. Rev.*, **109,** 1629–1653.

Leith, C., 1980: Nonlinear normal mode initialization and quasi-geostrophic theory. *J. Atmos. Sci.*, **37,** 958–968.

Machenhauer, B., and R. Daley, 1972: A baroclinic primitive equation model with a spectral representation in three dimensions. Rep. No. 4, Kobenhavns Universitet, Institut for Teoretisk Meteorologi.

——, and E. Rasmussen, 1972: On the integration of the spectral hydrodynamical equations by a transform method. Rep. No. 3, Kobenhavns Universitet, Institut for Teoretisk Meteorologi.

Ooyama, K., 1969a: Numerical simulation of the life cycle of tropical cyclones. *J. Atmos. Sci.*, **26,** 3–40.

——, 1969b: Numerical simulation of tropical cyclones with an axisymmetric model. *Proc. WMO/IUGG Symp. on Numerical Weather Prediction,* Tokyo, 1968, III: 81–88.

——, 1982: Conceptual evolution of the theory and modeling of the tropical cyclone. *J. Meteor. Soc. Japan,* **60,** 369–379.

——, 1984: A model for hurricane prediction. *Proc. of the 15th Technical Conference on Hurricanes and Tropical Meteorology.* Miami. Amer. Meteor. Soc., 580 pp.

Orszag, S. A., 1970: Transform method for the calculation of vector-coupled sums: Application to the spectral form of the vorticity equation. *J. Atmos. Sci.*, **27,** 890–895.

Schubert, W. H., and J. J. Hack, 1982: Inertial stability and tropical cyclone development. *J. Atmos. Sci.*, **39,** 1687–1697.

——, and ——, 1983: Transformed Eliassen balanced vortex model. *J. Atmos. Sci.*, **40,** 1571–1583.

——, ——, P. L. Silva Dias and S. R. Fulton, 1980: Geostrophic adjustment in an axisymmetric vortex. *J. Atmos. Sci.*, **37,** 1464–1484.

Simmons, A. J., and B. J. Hoskins, 1975: A comparison of spectral and finite difference simulations of a growing baroclinic wave. *Quart. J. Roy. Meteor. Soc.*, **101,** 551–565.

Temperton, C., 1984: Orthogonal vertical normal modes for a multilevel model. *Mon. Wea. Rev.*, **112,** 503–509.

Tribbia, J. J., 1981: Nonlinear normal-mode balancing and the ellipticity condition. *Mon. Wea. Rev.*, **109,** 1751–1761.

Yamasaki, M., 1968a: Numerical simulation of tropical cyclone development with the use of primitive equations. *J. Meteor. Soc. Japan,* **46,** 178–201.

——, 1968b: A tropical cyclone model with parameterized vertical partition of released latent heat. *J. Meteor. Soc. Japan,* **46,** 202–214.